THE JOURNAL OF PHYSICAL CHEMISTRY C

Article

Correlation Cataluminescence (CTL) Property with Reactivity of Hydrothermally Synthesized LaSrMnO Cubes and CTL as a Rapid Mode of Screening Catalyst

Fei Teng, Wenqing Yao, Yongfa Zhu, Mindong Chen, Ranhui Wang, Sun-il Mho, and Dennis Desheng Meng

J. Phys. Chem. C, **2009**, 113 (8), 3089-3095• DOI: 10.1021/jp711773w • Publication Date (Web): 30 January 2009

Correlation Cataluminescence (CTL) Property with Reactivity of Hydrothermally Synthesized $La_{0.8}Sr_{0.2}MnO_3$ Cubes and CTL as a Rapid Mode of Screening Catalyst

Fei Teng,*,†,‡,§ Wenqing Yao,‡ Yongfa Zhu,*,‡ Mindong Chen,† Ranhui Wang,† Sun-il Mho,|| and Dennis Desheng Meng*,§

Department of Chemistry, Tsinghua University, Beijing 100084, P. R. China, Department of Mechanical Engineering−Engineering Mechanics, Michigan Technological University, Houghton, Michigan 49931, School of Environmental Science and Engineering, Nanjing University of Information Science & Technology, Nanjing 210044, P.R. China, and Division of Energy System research, Ajou University, Suwon 443-749, Korea

Received: December 14, 2007; Revised Manuscript Received: December 18, 2008

$La_{0.8}Sr_{0.2}MnO_3$ cubes and nanoparticles were prepared by hydrothermal and citrate methods, respectively. Their cataluminescence (CTL) properties and catalytic reaction activities for CO were mainly investigated. The samples were characterized by XRD, SEM, TEM, LRS, BET, CO-TPD, O_2-TPD, and H_2-TPR, etc. It was found that both crystal structure and surface area of the catalyst play the important roles in CO oxidation. Before being calcined at high temperatures, $La_{0.8}Sr_{0.2}MnO_3$ nanoparticles showed the higher CTL intensity and catalytic activity for CO oxidation than the cubes, in which the effect of BET area of the catalyst on the catalytic properties is obvious; after being calcined at high temperatures, nevertheless, the cubes showed a higher CTL intensity and catalytic activity than the particles, in which the crystal structure played a significant role in CO oxidation. Most importantly, the CTL intensity of the catalyst was well correlated with the catalytic reaction activity (CO conversion or apparent reaction rate). A CTL mode could be used as a rapid method for screening catalyst activity.

Introduction

In 1976, cataluminescence phenomenon was first reported by Breysse et al. They observed that a weak catalytic luminescence phenomenon occurred during catalytic oxidation of CO on ThO_2 surface. This luminescence mode was defined as cataluminescence (CTL).[1] In a chemical reaction, the resulting molecular species are excited to an electronic excited state. While the exited molecular species fall to their ground states, a weak light is released. On a solid catalyst, CTL generally results from the interaction between gas and solid surface. At that time, however, the CTL phenomenon did not attract the attention of researchers. Since the 1990s, nanoparticles have attracted widespread attention because of their potential application in many areas, such as catalysis,[2,3] chemical and biochemical sensing,[4,5] and biological imaging.[6,7] Nanoparticles have provided new avenues to expand the analytical applications of this CTL mode of detection. McCord et al. found that the interaction of porous silicon with nitric acid or persulfate could result in an intense CTL, indicating that CTL is generated on the surface of nanoparticles.[8] The direct CTL reactions of gold nanoparticles with acidic permanganate, alkaline periodate and carbonate, or bis(2,4,6-trichlorophenyl)oxalate and hydrogen peroxide have also been examined but not yet applied to analysis.[9−11] Many investigations have indicated that CTL properties of nanoparticles could be potentially applied in the new fields. The different organic vapors can be discriminated from the different CTL responses over the nanoparticles.[12,13] To date, CTL properties of noble metals nanoparticles have been extensively researched. Since these noble metals are scarce in Nature and expensive, it is desirable to research CTL properties of inexpensive materials. Recently, Zhu et al.[14] have first researched CTL properties of organic vapor over the nanoparticles, including MgO (28 nm), TiO_2 (20 nm), Al_2O_3 (18 nm), Y_2O_3 (90 nm), $LaCoO_3$:Sr^{2+} (50 nm), and $SrCO_3$ (25 nm). Rakow et al.[15] indicated that these materials could be potentially used to fabricate a chip-mounted sensor array. Nakagawa et al.[16] have manufactured a γ-Al_2O_3 sensor to detect ethanol and acetone utilizing the combustibility of gas on the solid. Okabayashi et al.[17] have also manufactured a Dy-doped γ-Al_2O_3 sensor used for hydrocarbon gases. Zhang et al. have designed the high selectivity CTL sensors for ethanol, aldehyde, ammonia, sulfureted hydrogen, and butyl ketone.[14,18−20] They further reported that the sensor of ZrO_2 nanoparticles has a high CTL response to ethanol but has no response to hexane, cyclohexane, ethylene, hydrogen, ammornia, and nitrogen oxides. While Tb was doped, the sensibility of Tb−ZrO_2 sensor can be twice that of the undoped one. They have also manufactured MgO−Al_2O_3 (4:1 mol ratio) nanosensor, which has a high selectivity to butyl ketone.[21] On basis of the literature, CTL properties of many single oxide nanoparticles have been reported. Nevertheless, the practice applications of these single oxide nanoparticles are limited by their thermal and structure stabilities, since the stability of nanoparticles is poor and the crystal structure of single oxide is easy to vary at high temperatures.

It is well-known that perovskites (ABO_3) are some of the most active and stable catalysts for the removal of pollutants (CO, NO_x, and hydrocarbon).[22] To the best of our knowledge, the catalytic reaction properties of perovskites have been extensively researched. Their CTL properties, however, have been scarcely reported up to now. Besides, all previous reports on CTL properties of micro- or nanoparticles have described

* Corresponding authors. F.T.: tel, (+86)25-5873-1090; e-mail, tfwd@163.com. Y.Z.: tel, (+86)10-6278-7601; e-mail, zhuyf@mail.tsinghua.edu.cn. D.D.M.: tel, (+1)906-4873551; e-mail, dmeng@mtu.edu.

† Tsinghua University.

‡ Michigan Technological University.

§ Nanjing University of Information Science & Technology.

|| Ajou University.

10.1021/jp711773w CCC: $40.75
Published on Web 01/30/2009

either the emission of molecular species catalyzed by the particle surface or the emission from localized states (e.g., surface traps) in a semiconductor solid (i.e., the emitting state had no relationship to the quantum-confined orbitals).[8,18,23] Most of the research focused on CTL applications in analysis. However, CTL applications in catalysis have not been reported. Generally, the catalysts are selected by determining their reaction activities. This selection mode is generally time-consuming and tedious (from several to tens of hours). It is needed to design a new and rapid mode of catalyst selection. The CTL mode may be one of the most useful methods, because the measurement of CTL spectra can be fulfilled within a few minutes, and no expensive reaction equipment is needed. However, the CTL properties of gases on perovskites have been scarcely researched and the essence of the relationships between CTL mechanism and catalytic reaction have been scarcely disclosed.[24]

It is well-known that the properties of materials are more dependent on their size and the shape of particles. The CTL properties of spherical nanoparticles have been generally reported.[2−7,25,26] However, the CTL of $La_{0.8}Sr_{0.2}MnO_3$ cubes has not been reported up to now. In this work, we reported, for the first time, the CTL properties for CO over $La_{0.8}Sr_{0.2}MnO_3$ catalysts with different morphologics and crystal structures. The effects of surface area and crystal structure of the catalyst on CTL and catalytic reaction properties of CO oxidation were mainly investigated, and the correlation of CTL with catalytic reaction of the catalyst was elucidated.

Experimental Section

All the chemicals, which were analytical grade, were purchased from Beijing Chemicals Co. Ltd. in China and used without further purification. $La_{0.8}Sr_{0.2}MnO_3$ cubes and nanoparticles were synthesized by hydrothermal and citrate methods, respectively.

Synthesis of $La_{0.8}Sr_{0.2}MnO_3$ Cubes. $La_{0.8}Sr_{0.2}MnO_3$ cubes were synthesized by a hydrothermal method. Typically, a mixture solution was prepared by dissolving $La(NO_3)_3 \cdot 6H_2O$, $SrCl_2 \cdot 6H_2O$, $KMnO_4$, and $MnCl_2 \cdot 4H_2O$ in deionized water. Then, KOH was added to the aqueous solution under ultrasonic stirring. The compositions of chemicals held the ratios of 7/3/2/8/1250/3256 ($Mn^{2+}/MnO_4^+/Sr^{2+}/La^{3+}/KOH/H_2O$). The mixture was poured into a Teflon vessel and subjected to a hydrothermal treatment at 240 °C for 24 h. After cooling to room temperature naturally, the solids were separated and washed several times with deionized water. Finally, the sample was washed with 0.1 M acetic acid solution so as to remove the impurities, and the solids were dried at 80 °C in an oven.

Synthesis of $La_{0.8}Sr_{0.2}MnO_3$ Nanoparticles. $La_{0.8}Sr_{0.2}MnO_3$ nanoparticles were prepared by a citrate method. The mixed solution was prepared by dissolving $La(NO_3)_3 \cdot 6H_2O$, $SrCl_2 \cdot 6H_2O$, $MnCl_2 \cdot 4H_2O$, and citric acid (CA) in deionized water, in which the molar ratios of La/Sr/Mn/CA were kept at 0.8/0.2/1/4. The resulting solution was evaporated at 80 °C to form a gel. The obtained spongy material was crushed and calcined at 600 °C for 5 h under flowing air.

In order to investigate the stability of catalysts, the as-prepared catalysts were further calcined in the temperature range of 600−800 °C for 48 h in air.

Characterization. The sample was characterized by XRD (Rigaku D/MAX-RB X-ray powder diffractometer), using graphite-monochromatized Cu Kα radiation ($\lambda = 0.154$ nm), operating at 40 kV and 50 mA. The patterns were scanned from 10° to 70° (2θ) at a scanning rate of 1° min^{-1}. A nitrogen adsorption isotherm was determined at −196 °C on a Micromeritics ASAP2010 gas adsorption analyzer. The sample was degassed at 250 °C for 5 h before the measurement. Surface area was calculated by the BET (Brunauer−Emmett−Teller) method. The morphology of the catalyst was observed on a TEM (JEOL 200CX) instrument with an accelerating voltage of 200 kV. The powders were ultrasonically dispersed in ethanol and then deposited on a thin amorphous carbon film supported by a copper grid. The morphology and composition of the sample were also characterized by SEM (KYKY 2800). The acceleration voltage was 15 keV and the current was 1.2 nA. ICP (inductively coupled plasma, Thermo Electron Corp., IRIS Intrepid II XSP) was used for the determination of metal element concentration. Raman spectra were measured at room temperature using a Jobin Yvon/Atago-Bussan T-64000 triple spectrometer with liquid nitrogen cooled CCD detector. Acquisition time was between 800 and 1200 s. The green line ($\lambda = 514.5$ nm) of an Ar^+ laser was used to excite the Raman spectra, using a laser beam power of 20 mW on the sample. Measurements were carried out under the microscope, using a 90 microscopy objective, and the laser spot size was around 1−2 μm. Raman measurements covered the range between 100 and 800 cm^{-1}. To obtain a high signal-to-noise ratio, Raman spectrum was the average of five successive scans obtained at a spectral resolution of 2 cm^{-1}.

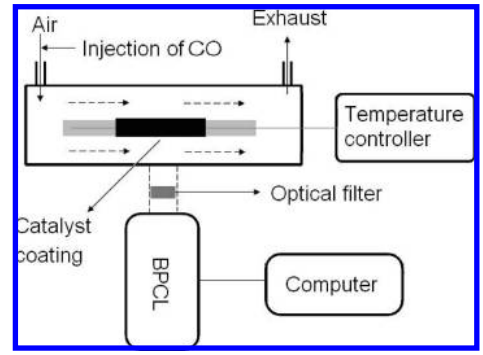

Figure 1. Sketched diagram of CTL test system.

Cataluminescence (CTL) Measurement. The consequent CTL intensity was directly measured with a BPCL ultraweak chemiluminescence analyzer (made by the Biophysics Institute of Chinese Academy of Science in China). The schematic diagram of the CTL system was shown in Figure 1. Typically, 0.02 g of the catalyst powder was mixed with absolute ethanol to prepare a slurry, and the slurry was coated on the surface of the heating tube and then it was dried under an infrared lamp for 30 min to form a coating. In order to control the thickness of the coating, the same procedure was repeated for two times. The mass of the coating was weighed in the range of 0.010 ± 0.001 g. The sensor was put into a quartz tube with the inner diameter of 12 mm. The CTL intensity of CO oxidation over the catalyst was determined with the bandpass filter of 640 nm by injecting a pulse of 50 mL of CO (>99.0%) into an air carry gas with a flow rate of 100 mL min^{-1}. The blank measurement was also performed under heating of the oxide material in the absence of CO or heating the mixed gases of CO and air but without adding the catalyst.

Catalytic Oxidation of CO. The oxidation of CO was carried out in a conventional flow system at atmospheric pressure. The catalyst (0.1 g) was loaded in a quartz reactor (inner diameter 5 mm), with quartz beads packed at both ends of the catalyst bed. The thermal couple was placed in the catalyst bed to monitor the reaction temperature since CO oxidation is an exothermic reaction. Before each run, the catalyst was flushed

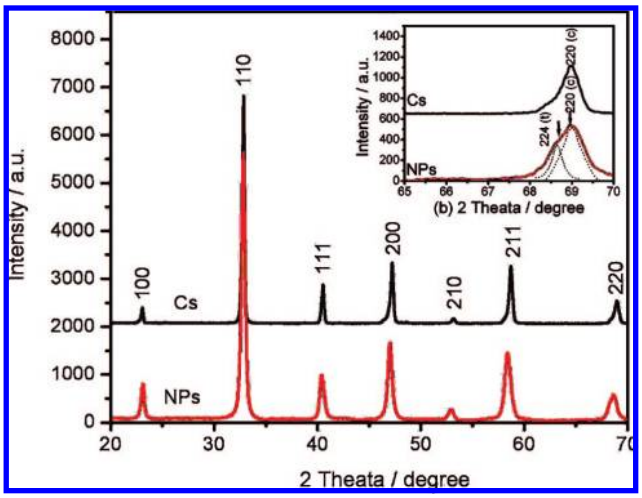

Figure 2. XRD patterns of $La_{0.8}Sr_{0.2}MnO_3$ catalysts: Cs, cubes synthesized by hydrothermal method; NPs, nanoparticles prepared by the citrate route.

with air (100 mL min^{-1}) at 500 °C for 1 h in order to remove adsorbed species from the surface and then cooled to 30 °C. A gas mixture of 2 vol % CO and 98 vol % air was fed to the catalyst bed at a flowing rate of 100 mL min^{-1}. The inlet and outlet gas compositions were analyzed by an online gas chromatograph with a GDX-403 GC-column (1.5 m × 4 mm) at 100 °C and a hydrogen flame ionization detector (FID).

CO-TPD, O_2-TPD, H_2-TPR, and TPSR experiments are outlined in the Supporting Information.

Results

XRD, SEM, and TEM of the Samples. Figure 2 gives the typical XRD patterns of $La_{0.8}Sr_{0.2}MnO_3$ cubes (Cs) and nanoparticles (NPs). All the diffraction peaks can be well indexed to a pure perovskite structure with a high crystallinity, and no peak shift can be observed for both samples. The XRD patterns of Cs can be indexed to a primitive cubic unit cell [space group *Pm*3*m*, $a = 0.3841(4)$ nm], in agreement with the lattice parameter of bulk material. In order to investigate their structure differences, a wide-angle scanning was performed in the range from 65° to 70° (see the inset of Figure 2). It can be observed that a peak broadening has taken place for NPs, compared with Cs. This may indicate that the crystal size of NPs is smaller than that of Cs. Further, although the peak splitting was reduced to some extent due to the small crystal size of NPs, the {220} peak splitting can still be discerned. The {224} peak appears, which is closely related to a tetragonal structure [space group *I*4/*mcm*, $a = 0.54806(3)$ nm, $c = 0.77206(6)$ nm]. The tetragonal polymorph resulted from the distortion of a cubic structure. The distorted structure might be due to the small size of the crystals and a high surface strain.[27] It could be assumed that NPs have an average structure of *I*4/*mcm* and *Pm*3*m*. NPs contained 80% cubic and 20% tetragonal polymorphs by calculation from their peak intensities based on Rietveld refinements. It could be concluded that both samples have different crystal structures, which will be further confirmed by LRS (see the latter part). Woodward et al. previously also reported that the $La_{0.8}Sr_{0.2}MnO_3$ crystals prepared by the ceramic method were composed of cubic and tetragonal polymorphs.[28] The contrast experiment showed that if not washed with the dilute acetic acid solution, the hydrothermally synthesized sample always contained a small quantity of $La(OH)_3$ impurities (not shown).

Figure 3 shows the morphologies of both samples. Cs sample consists of the highly regular cubes with a wide size distribution (0.1−2 μm) (Figure 3a). The bright spots of SAED patterns (the inset of Figure 3b) confirm the single crystal properties of Cs. Figure 3c,d showed that NPs sample consists of polycrystalline nanoparticles with diameters of 30−50 nm, which are larger than their average size (about 25 nm) calculated using the Scherrer equation based on the peak of {110}. ICP elemental analysis confirmed that the compositions of both samples were close to the stoichiometric ratios of $La_{0.8}Sr_{0.2}MnO_3$ (La/Sr/Mn = 0.77/0.19/1 for Cs and La/Sr/Mn = 0.75/0.18/1 for NPs). The mass ratios of Mn in Cs and NPs were accurate within ±5%.

CTL Properties of the Samples. We determined CTL intensities of both samples at different test temperatures (Figure S1, Supporting Information). It can be observed that CTL intensity increases with the temperature over both catalysts. In our experiments, while heating the catalysts in the absence of CO or heating the flowing mixed gases of both CO and air at 200 °C, no emission of thermoluminescence can be observed. Figure 4 gives the typical CTL spectra of CO over the catalysts at 200 °C. It could be observed that CTL intensity (2.5×10^4 au) of Cs is lower than that (3.4×10^4 au) of NPs. CTL spectra indicated that more CO molecules were oxidized into CO_2 molecules over NPs than over Cs. After being calcined at 750 °C, nevertheless, the CTL intensity (2.3×10^4 au) of Cs (Cs750) was higher than that (1.75×10^4 au) of NP (NPs750). It has been reported that the CTL intensity is proportional to the concentration of CO_2.[1,30−32]

The catalyst properties including crystal structure, composition, BET surface area, and/or particle size, etc. have an important influence on CO oxidation. Because of their same compositions, the influences of the BET surface area and/or particle size and crystal structure of the catalysts on CO oxidation are mainly considered. It is generally accepted that a catalyst with a high surface area could provide more active sites than that with a small surface area, which favors the adsorption and activation of the reacting molecules. NPs have a surface area (18.8 $m^2\ g^{-1}$) higher than the Cs (7.3 $m^2\ g^{-1}$). More CO_2 molecules can be produced over NPs than over Cs; therefore, NPs has a higher CTL intensity. Note that the thermal stability of a catalyst is an important factor for the practice applications. The thermal stabilities of the catalysts were investigated by calcining at a high temperature for a long duration. After calcination at 750 °C for 48 h in air, the BET areas of NPs750 and Cs750 are 10.5 and 6.5 $m^2\ g^{-1}$, respectively. The surface area of Cs750 decreased by 16%, but that of NPs750 decreased by 44%. The catalysts showed different extents of sintering. As shown in Figure S2 (Supporting Information), SEM images confirmed that NPs750 sintered severely and grew into agglomerates. Nevertheless, the cubes almost maintained their cubic morphologies. XRD patterns confirmed that the compositions of both samples did not vary. It is obvious that the single crystal cubes had a higher thermal stability than the nanoparticles. The high thermal stability of the cubes could be closely related to the unique cube morphology and the low surface energy.[33] Two important factors should be considered. First, the surface-to-volume ratio of the cubes is lower than that of the nanoparticles, and thus there is a smaller driving force to sinter for the cubes. Second, the perfect single crystal structure may also contribute the stability of Cs. It could be observed that, after being calcined at 750 °C, the CTL intensity of the cube sample decreased slightly, but that of the nanoparticles decreased greatly (to an extent of about 50%). Although the BET area of Cs is smaller than that of NPs750, the CTL intensity of Cs750 was higher than that of NPs750. Their different CTL intensities cannot be understood by their BET areas, because Cs750 has a lower BET area than NPs750. The high CTL

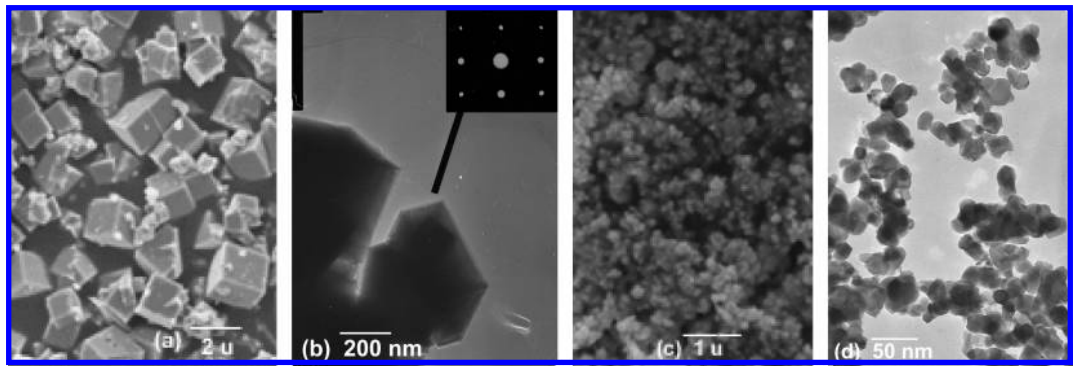

Figure 3. SEM and TEM micrographs of $La_{0.8}Sr_{0.2}MnO_3$ catalysts: (a, b) Cs, the inset of SAED; (c, d) NPs.

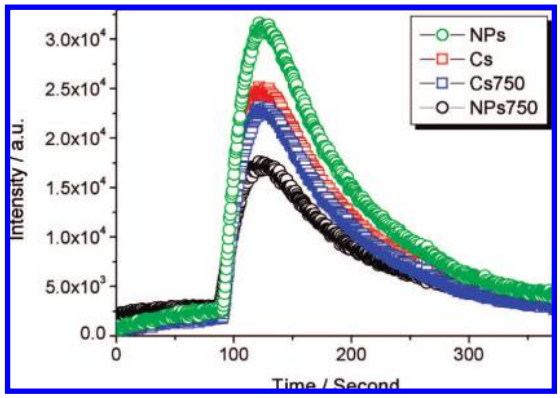

Figure 4. CTL spectra of $La_{0.8}Sr_{0.2}MnO_3$ catalysts and Cs750 and NPs750 (Cs and NPs calcined at 750 °C for 48 h in air, respectively). Determination conditions: injection pulse of CO = 50 mL, flow rate = 100 mL min^{-1}, T = 200 °C.

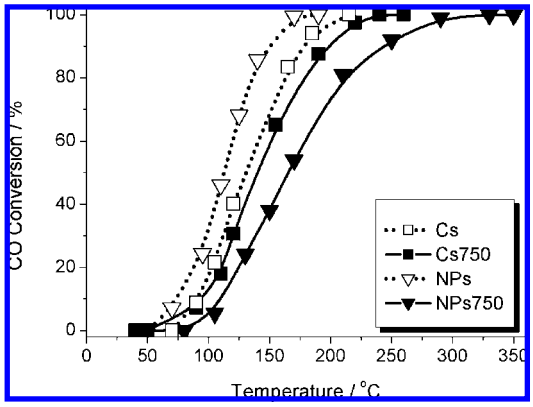

Figure 5. Activities of CO oxidation over $La_{0.8}Sr_{0.2}$ MnO_3 catalysts: 100 mL min^{-1} flow rate, 2 vol % CO.

intensity of Cs750 may be closely related to its cubic structure, which is discussed in the latter.

Catalytic Activities of the Samples. Figure 5 gives the reaction activities of CO oxidation over the catalysts. The complete oxidations of CO over NPs and Cs were achieved at 190 and 215 °C, respectively. However, the complete oxidations of CO over NPs750 and Cs750 were achieved at 310 and 235 °C, respectively. It is clear that, after high-temperature calcination, the reaction activity of the nanoparticles decreased significantly, but that of the cubes decreased only slightly.

The CO-TPD (temperature-programmed desorption) was performed to explore the adsorption types and strength of CO on $La_{0.8}Sr_{0.2}MnO_3$ catalysts. While CO adsorbed on the catalyst, a significant portion of CO desorbed from the catalyst in the form of CO_2. TPD profiles reveal the presence of at least three different types of adsorbed CO with significantly different adsorption strength and reactivity, as deduced from the dramatically different desorption temperatures (Figure S3, Supporting Information). In CO_2-TPD profiles, four desorption peaks of CO_2 are observed at 150, 320, 475, and 640 °C over NPs, and three peaks are observed at 170, 465, and 650 °C over NPs750. On the other hand, three desorption peaks of CO_2 are observed at 145, 350 and 680 °C over Cs, and two peaks are observed at 400 and 680 °C over Cs750 (Figure S3a, Supporting Information). In CO-TPD profiles, four desorption peaks of CO are observed at 140, 305, 470, and 650 °C over NPs, and two peaks are observed at 460 and 650 °C over NPs750, respectively. Nevertheless, three desorption peaks of CO are observed at 145, 345, and 645 °C over Cs, and two peaks are observed at 415 and 650 °C for the Cs750 (Figure S3b, Supporting Information). The quantitative analysis results (Table S1 of Supporting Information) show that the total desorbed amount (135.1 μmol g^{-1}) of carbonaceous species on NPs is larger than that (48.9 μmol g^{-1}) on Cs. After being calcined at 750 °C, however, the total desorbed amount (40.6 μmol g^{-1}) of carbonaceous species on NPs750 is slightly smaller than that (42.7 μmole g^{-1}) on Cs750. It is clear that the total desorbed amount of carbonaceous species on the nanoparticles significantly decreased more than those on the cubes. This may be related to the sintering of the catalysts. After being calcined at high temperatures, the severe sintering of active sites occurred due to the high surface energy of NPs, but Cs sintered only slightly. Here, the carbon deposited on the catalyst surface is neglected and the total desorption amount of both CO and CO_2 is used to express the adsorption amount of CO, since the real adsorption amount of CO cannot determined. We can assume that the CO adsorption amount on NPs750 was reduced significantly.

It is noted that the steady-state catalytic measurements were made at temperatures lower than 350 °C. Therefore, CO-TPD is not enough to explore the catalytic oxidation and TPSR experiments (reaction of adsorbed CO with gaseous oxygen) were further performed to explore the reactivity of the catalysts. Figure S4 (Supporting Information) shows TPSR profiles of CO oxidation over NPs750 and Cs750. The onset temperature for the catalytic oxidation over NPs750 was found to be about 130 °C, and the maximum reaction rate was achieved at about 330 °C. The onset temperature for the catalytic oxidation over Cs750 was about 100 °C and the maximum reaction rate was achieved at 250 °C, which are lower than those over NPs750, respectively. TPSR results also indicate that CO oxidation over Cs750 is faster than over NPs750. It is understandable that probably only weakly adsorbed CO (the one desorbing at low temperatures)

TABLE 1: BET Areas, Activities and Reaction Rates of CO Oxidation over $La_{0.8}Sr_{0.2}MnO_3$ Catalysts

catalysts	SA[a] ($m^2\ g^{-1}$)	$T_{10\%}$[b] (°C)	$T_{50\%}$[b] (°C)	$T_{100\%}$[b] (°C)	reaction rate at 200 °C (10^{-3} mol $h^{-1}\ g^{-1}$)
Cs	7.3	90	130	215	17.89
NPs	18.8	70	110	190	20.68
Cs750	6.5	95	140	235	14.94
NPs750	10.5	110	165	310	7.05

[a] SA, surface area calculated by BET method. [b] $T_{10\%}$, $T_{50\%}$,$T_{95\%}$, the temperatures at 10%, 50%, 100% CO conversion, respectively.

should participate in the reaction cycle, because the steady-state catalytic measurements were made at temperatures lower than 350 °C (shown in Figure 5).

O_2-TPD results are given in Figure S5 and Table S2 (Supporting Information). The adsorption of oxygen on NPs750 and Cs750 are similar. Note that this difference is not significant. Although the BET area of NPs750 is higher than that of Cs750 (Table 1), Cs750 showed a higher CTL intensity and a higher activity for CO oxidation than NPs750. This may indicate that the crystal structure plays an important role in CO oxidation due to the small difference of their BET area.

Laser Raman Spectroscopy (LRS) of the Samples. To explore the catalyst structures, Raman spectra of $La_{0.8}Sr_{0.2}MnO_3$ catalysts were determined. LRS spectroscopy is very sensitive not only to the structural phase transition but also to the subtle changes in the local structure or the electronic states.[34,35] LRS spectra of the doped $La_{1-x}A_xMnO_3$ crystals are composed of two parts: the first part is related to the distorted noncubic perovskite structure following the selection rules for first-order Raman scattering; the second part is mainly due to the density of vibration states and is classified as second-order Raman scattering. As shown in Figure 6a,b, the Raman spectrum of NPs750 showed three peaks (185, 465, 650 cm^{-1}). The 185 and 465 bands denote the polarization properties of A_{1g} (resulting from the motion of the oxygen ions) and B_{1g} (mainly involving oxygen motions) symmetry vibration modes. These bands, following the selection rules for first-order Raman scattering, are related to the distorted noncubic perovskite structure (caused by the ion substitution for A-site cations along the certain directions and/or by tilting of MnO_6 octahedral). Compared with the undoped $LaMnO_3$ compound, however, these bands are weaker.[36] Generally, the Jahn−Teller deformation of the $Mn^{3+}O_6$ octahedra lowers the local atomic site symmetry and the new bands can be considered as Jahn−Teller distortion activated modes.[37] Since the partial substitution of Sr for La reduces the deviations from an ideal cubic structure, the presence of Mn^{4+} generated by the doped Sr reduces the static Jahn−Teller distortion. The 650 cm^{-1} band, which is much weaker than those of undoped $LaMnO_3$, is mainly related to a disordered perovskite structure.[38] The band correlates mainly with the Jahn−Teller effect or the density-of-states of the oxygen phonon, following the selection rules for second-order Raman scattering. Further, considering the polarization properties of the corresponding Raman tensor components, the observed spectrum of NPs750 seems to be more consistent with a distorted D^5_{4h} tetragonal structure.[38,39] For an average structure, the new Raman bands, related to the local Jahn−Teller distortions, will appear in the three intervals (about 180−300, 400−520, and 580−680 cm^{-1}), which are typical Raman spectra of perovskite structures in the nearly cubic phase.[40] It could be deduced that $La_{0.8}Sr_{0.2}MnO_3$ nanoparticles share an average structure of cube (*Pm*3*m*) with tetragon (*I*4/*mcm*). The LRS results are consistent with those from XRD patterns. Nevertheless, $La_{0.8}Sr_{0.2}MnO_3$ cubes do not show the 185 and 465 cm^{-1} bands (the first-order Raman scattering bands), which resulted from the smaller Jahn−Teller distortion of the ideal cubic structure. In an ideal cubic structure (*Pm*3*m*), all lattice sites have inversion symmetry, and the first-order Raman scattering is forbidden.[42] Also, the cube sample does not show the 650 cm^{-1} band. The disappearance of the high-wavenumber broad peaks denotes that the cubes have an idea cubic structure.[41] As a result, the MnO_6 octahedron distortion by Mn^{3+} Jahn−Teller effect and the number of the oxygen vacancies in the single crystal cubes are smaller than those in the nanoparticles.

Discussion

Effects of Crystal Structure and BET Area of the Catalyst on CO Oxidation. It can be expected that both the BET area and crystal structure of the catalyst have an important influence on the adsorption of reacting molecules and the electron transfer among Mn^{4+}−O−Mn^{3+}. For the CO chemisorption on manganites, CO molecules would attach to the coordination sites of MnO_6 (unsaturated metal sites, Mn^{3+}), where some oxygen ligands are missing. It seems that CO and coordination sites of MnO_6 function as Lewis base and Lewis acid, respectively. The chemisorption occurs by donation of 5σ electrons in CO to Lewis acid sites of MnO_6. The Mn^{4+}−Mn^{3+} pairs on the surface or near the surface may have a significant influence on activity. The high percentage of Mn^{4+}−Mn^{3+} pairs favors the surface reaction. Such pairs might be particularly favorable for adsorption−desorption flip-flops, when remaining isolated from neighboring pairs. In such a case, charge transfer from one ion to its partner and vice versa should be easy, since there is no reason for the electron to stay localized in one or the other cation. Another contribution to the catalytic activity, which might be also related to the unusual Mn^{3+} oxidation state, is the occupancy of e_g and t_{2g} orbitals. For the influence of B cations of ABO_3 on CO oxidation, previous studies have shown that the maximum activity is attained under an occupation of the e_g levels of less than one electron, while the t_{2g} electrons are half-filled or totally filled.[42] In an ideal cubic perovskite, the Mn^{3+}−O−Mn^{4+} angle is equal to 180 °C and no tilting of octahedral occur. In the case of an electronic hopping mechanism (Figure 6c), the presence of Mn^{3+}−O−Mn^{4+} bond angles close to 180° optimizes the electron transfer process; the cubic surface should make the hopping process easier, since possible carriers' localization phenomena should be highly minimized.[41] In a manganite perovskite, the presence of Mn ions with different oxidation states is of crucial importance for the transport properties and in turn for the catalytic activity. When Mn^{3+} and Mn^{4+} are simultaneously present, it has been shown that an electron hopping between those two ions with intervening oxygen is the basic conduction mechanism. The hopping is favored if the Mn^{3+}−O−Mn^{4+} angle in the cubic structure is of 180°.[43] This may greatly accelerate the electron transfer and the oxidation of CO molecules. For the nanoparticles with an average structure, however, the present distorted tetragon structure does not favor electron transfer. Further, H_2-TPR results confirmed that Cs750 is easier to reduce than NPs750 (Figure S6 and Table S3, Supporting Information). As a result, CO oxidation over Cs750 is faster than over NPs750. TPSR results also indicate that CO oxidation over Cs750 is faster than over NPs750.

It is noted that both crystal structure and BET area of the catalyst play an important role in CO oxidation. Before being calcined at high temperatures, the difference in BET areas of the catalysts was large enough, the effect of BET area on CO oxidation being more significant than the crystal structure. After being calcined at high temperature, however, the difference in BET areas of the catalysts was small, and the effect of crystal structure (especially Jahn−Teller distortion) on CO oxidation became significant.

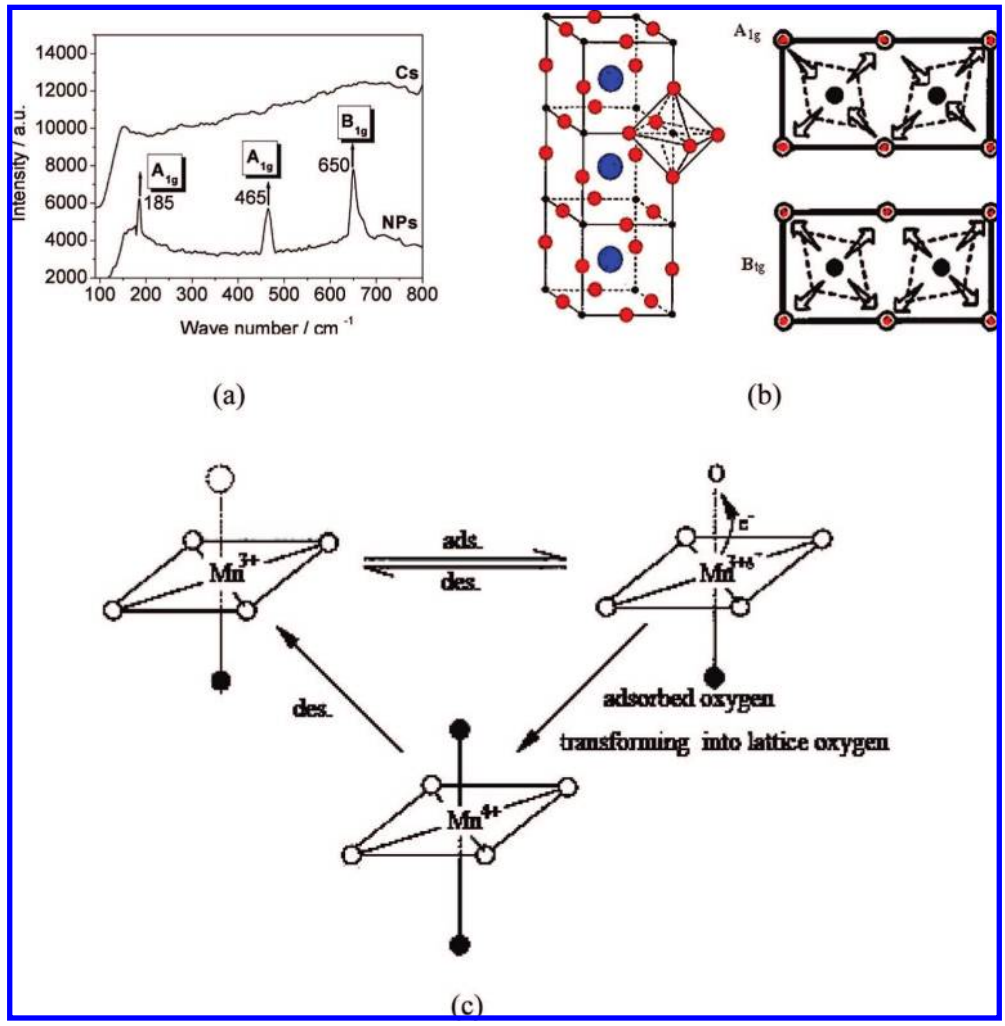

Figure 6. Raman spectra (a), crystal structure (b), and electron transfer process (c) of $La_{0.8}Sr_{0.2}MnO_3$ catalysts: A_{1g}, Raman scattering mode resulting from the asymmetry motion of the oxygen ions; B_{1g}, symmetry vibration modes mainly involving oxygen motions.

A Rapid CTL Detection Mode. Concerning catalytic mechanism, the catalytic oxidation of CO has been considered as the so-called suprafacial catalytic process,[44] in which the crystal structure and the surface properties of the catalyst could play an important role. Tascon et al.[45] proposed the following catalytic mechanism of CO oxidation on $LaCoO_3$:

$$O_2(g) \rightarrow O_2(ads) \rightarrow 2O(ads)$$
$$CO(g) \rightarrow CO(ads)$$
$$CO(ads) + 2O(ads) \rightarrow CO_3(ads)$$
$$CO_3(ads) \rightarrow CO_2(ads) + O(ads)$$
$$CO_2(ads) \rightarrow CO_2(g) \quad (1)$$

The authors suggested that cobalt and oxygen sites act as adsorption and activation centers for CO and O_2, respectively. The adsorbed CO on cobalt site reacts with the lattice oxygen, whereas the chemisorbed oxygen transforms into the lattice oxygen to reinforce the consumed lattice oxygen.[46] It has been proposed that the oxygen transformation occurs in CoO_6 octahedral.[47] Similarly, the manganese site is the active center for CO and the lattice oxygen is active oxygen species. The adsorption of reacting molecules on the catalyst played an important role in CO oxidation.

While CO molecules are oxidized into CO_2 molecules on the surface of the catalyst, the amounts of energy are released. These CO_2 molecules would absorb the released energy, and the electrons in CO_2 molecule would be excited. As a result, CO_2 molecules at the electronic ground-state become the electronic excited molecules. While the electronic excited CO_2 molecules decay to the electronic ground state, a weak luminescence would be emitted.[1,29] CTL reaction can be represented with the following formula:

$$CO(ads) + O \rightarrow {}^*CO_2(ads) \rightarrow CO_2 + h\nu \quad (2)$$

CTL intensity is obtained by measuring the quantum number of the generated photons, i.e., CTL intensity is directly proportional to the photonic quantum number. The more CO_2 molecules that are produced, the more CO_2 molecules that would be electronically excited through absorbing the released energy. While these electronically excited CO_2 molecules decay to the ground state, the more photonic quantum number is generated. CTL intensity may be proportional to CO_2 concentration or the apparent reaction rate (mol g^{-1} s^{-1}). The apparent reaction rate is closely correlated to the textural properties (BET area) and intrinsic properties of the catalysts.

It seems that the CTL and catalytic activity (CAA, CO conversion) essentially result from one catalytic reaction process. The CTL−CAA plot is given in Figure S7 (Supporting Information). It can be observed that CTL intensity is directly proportional to CAA, although they were not measured under the completely same conditions. Moreover, NPs and Cs catalysts were calcined

at different temperatures (600−800 °C/48 h). We have determined their CTL intensities and CAA, which are given in Figures S8 and S9 and Table S4 (Supporting Information). The results also showed that the order of CTL intensities is consistent with that of their activities. In our previous studies, we have also found the parallel correlations between CTL and catalytic activity.[48,49] We cannot determine CTL and CAA under the completely same conditions; they were obtained at different CO concentration but at the same flow rate. However, this parallel relationship between CTL and CAA indicates that the CTL could be potentially used for screening the activities of the catalysts.

We could develop a new CTL-typed screening method, which is simple and rapid for screening the catalytic activities of the catalysts. This technique would be potentially applied to explore the new catalysts. When we select the excellent catalysts from thousands of materials, it is generally time-consuming, tiring, and expensive to determine their activities by a catalytic reaction. The catalyst selection is still a challenge to us. The CTL mode is facile, rapid, and low-cost, since no expensive equipment is needed and the test could be completed with success within a few minutes. Since CTL and CAA of $La_{0.8}Sr_{0.2}MnO_3$ cubes can be maintained after being calcined at high temperatures for a long duration, the cubes can be used to fabricate a stable gas sensor with a rapid response. It should be noted that the CTL method is possibly insufficient for judging the selectivity of different gases, which needs further research.

Conclusions

$La_{0.8}Sr_{0.2}MnO_3$ cubes can be synthesized by a hydrothermal method. Both crystal structure (Jahn−Teller distortion) and BET area of the catalyst played an important role in CO oxidation. A fast electron transfer in cubic structure and a high BET area contribute to catalytic oxidation of CO. The CTL intensity of the catalyst well-correlated with its catalytic activity, and CTL could be a rapid and effective means for screening the activity of the catalyst.

Acknowledgment. This work is financially supported by the National Basic Research Program of China (Grant 2007CB613303), Chinese Postdoctoral Science Foundation (Grant 20060390057), Chinese National Science Foundation (Grants 20433010 and 20571047), Michigan Tech Faculty Startup Fund (N4901928249), and the Korea Research Foundation Grant (KRF-2007-412-J04003).

Supporting Information Available: The experiments and results of CO-TPD, O_2-TPD, H_2-TPR, and TPSR; the influence of operation temperature on CTL intensity; SEM micrographs and XRD patterns of the catalysts after being calcined at 750 °C for 48 h; correlation plot of CTL with CAA of Cs; CTL, CAA, and BET areas of NPs and Cs after being calcined at different temperatures. This material is available free of charge via the Internet at http://pubs.acs.org.

References and Notes

(1) Breysse, M.; Claudel, B.; Faure, L.; Guenin, M.; Williams, R. J. J.; Wolkenstein, T. J. *J. Catal.* **1976**, *45*, 137.
(2) Daniel, M.-C.; Astruc, D. *Chem. Rev.* **2004**, *104*, 293.
(3) Burda, C.; Chen, X.; Narayanan, R.; El-Sayed, M. A. *Chem. Rev.* **2005**, *105*, 1025.
(4) Aslan, K.; Lakowicz, J. R.; Geddes, C. D. *Anal. Chem.* **2005**, *77*, 2007.
(5) Elghanian, R.; Storhoff, J. J.; Mucic, R. C.; Letsinger, R. L.; Mirkin, C. A. *Science* **1997**, *277*, 1078.
(6) Santra, S.; Dutta, D.; Walter, G. A.; Moudgil, B. M. *Technol. Cancer Res. Treat.* **2005**, *4*, 593.
(7) El-Sayed, I. H.; Huang, X.; El-Sayed, M. A. *Nano Lett.* **2005**, *5*, 829.
(8) McCord, P.; Yau, S. L.; Bard, A. J. *Science* **1992**, *257*, 68.
(9) Zhang, Z.; Cui, H.; Shi, M. *Phys. Chem. Chem. Phys.* **2006**, *8*, 1017.
(10) Cui, H.; Zhang, Z.; Shi, M. *J. Phys. Chem. B* **2005**, *109*, 3099.
(11) Cui, H.; Zhang, Z.; Shi, M.; Xu, Y.; Wu, Y. *Anal. Chem.* **2005**, *77*, 6402.
(12) Poznyak, S. K.; Talapin, D. V.; Shevchenko, E. V.; Weller, H. *Nano Lett.* **2004**, *4*, 693.
(13) Powe, A. M.; Fletcher, K. A.; St Luce, N. N.; Lowry, M.; Neal, S.; McCarroll, M. E.; Oldham, P. B.; McGown, L. B.; Warner, I. M. *Anal. Chem.* **2004**, *76*, 4614.
(14) Zhu, Y. F.; Shi, J.; Zhang, Z.; Zhang, C.; Zhang, X. R. *Anal. Chem.* **2002**, *74*, 120.
(15) Rakow, N. A.; Suslick, K. S. *Nature* **2000**, *406*, 710.
(16) Nakagawa, M.; Yamamoto, I.; Yamashita, N. *Am al. Sci.* **1998**, *14*, 209.
(17) Okabayashi, T.; Fujimoto, T.; Yamamoto, I.; Utsunomiya, K.; Wada, T.; Yamashita, Y.; Yamashita, N.; Nakagawa, M. *Sens. Actuators B* **2000**, *64* (1−3), 54.
(18) Zhang, Z. Y.; Zhang, C.; Zhang, X. R. *Analyst* **2002**, *127* (6), 792.
(19) Shi, J. J.; Li, J. J.; Zhu, Y. F.; Fan, W.; Zhang, X. R. *Acta Anal. Chim.* **2002**, *466* (1), 69.
(20) Rao, Z. M.; Shi, J. J.; Zhang, X. R. *Acta Chim. Sin.* **2002**, *60* (9), 1668.
(21) Zhou, K. W.; Zhang, X. R. *Chin. J. Anal. Chem* **2004**, *32* (1), 25.
(22) Seiyama, T. *Catal. Rev. Sci. Eng.* **1992**, *34* (4), 281.
(23) Corralles, T.; Peinado, C.; Allen, N. S.; Edge, M.; Sandoval, G.; Catalina, F. J. *Photochem. Photobiol. A* **2003**, *156*, 151.
(24) Ye, Q.; Gao, Qi.; Zhang, X. R.; Xu, B. Q. *Acta Chim. Sin.* **2006**, *24* (8), 751.
(25) Stuart, D. A.; Haes, A. J.; Yonzon, C. R.; Hicks, E. M.; Duyne, R. P. V. *IEE Proc.: Nanobiotechnol.* **2005**, *152*, 13.
(26) West, J. L.; Halas, N. J. *Annu. Rev. Biomed. Eng.* **2003**, *5*, 285.
(27) Bindu, R.; Pandey, S. K.; Kumar, A.; Khalid, S.; Pimpale, A. V. *J. Phys.: Condens. Matter* **2005**, *17*, 6393.
(28) Woodward, P. M.; Vogt, T.; Cox, D. E.; Arulraj, A.; Rao, C. N. R.; Karen, P.; Chettham, A. K. *Chem. Mater.* **1998**, *10*, 3652.
(29) Nakao, K.; Ito, S.; Tomishige, K.; Kunimori, K. *J. Phys. Chem. B* **2005**, *109*, 17553.
(30) Shi, J. J.; Zhu, Y. F.; Zhang, X. R.; Baeyens, W. R. G.; Garcia-Campana, A. M. *Trends Anal Chem.* **2004**, *23*, 351.
(31) Nakagawa, M.; Okabayashi, T.; Fujimoto, T.; Utsunomiya, K.; Yamamoto, I.; Wada, T.; Yamashita, Y.; Yamashita, N. *Sens. Actuators B* **1998**, *51*, 159.
(32) Wang, X.; Na, N.; Zhang, S. C.; Wu, Y. Y.; Zhang, X. R. *J. Am. Chem. Soc.* **2007**, *129*, 6062.
(33) Zhang, T.; Jin, C. G.; Qian, T.; Lu, X. L.; Bai, J. M.; Li, X. G. *J. Mater. Chem.* **2004**, *14*, 2787.
(34) Gupta, R.; Sood, A. K.; Mahesh, R.; Rao, C. N. R. *Phys. Rev. B* **1996**, *54*, 14899.
(35) Podobedov, V. B.; Weber, A.; Romero, D. B.; Rice, J. P.; Drew, H. D. *Bull. Am. Phys. Soc.* **1997**, *42*, 341.
(36) Podobedov, V. B.; Weber, A.; Romero, D. B.; Rice, J. P.; Drew, H. D. *Phys. Rev.* **1998**, *58*, 43.
(37) Goodenough, J. B.; Wold, A.; Arnott, R. J.; Menyuk, N. *Phys. Rev.* **1961**, *124*, 373.
(38) Podobedov, V. B.; Weber, A.; Romero, D. B.; Rice, J. P.; Drew, H. D. *Solid State Commun.* **1998**, *105*, 589.
(39) Milko, N. I.; Miroslav, V. A. *J. Raman Spectrosc.* **2001**, *32*, 805.
(40) Liarokapis, E.; Leventouri, T.; Lampakis, D. *Phys. Rev. B* **1999**, *60*, 12758.
(41) Malavasi, C.; Tealdi, G.; Flor, G.; Chiodelli, V.; Cervetto, A.; Montenero, M. *Sens. Actuat. B* **2005**, *105*, 407.
(42) Belessi, V. C.; Ladavos, A. K.; Pomonis, P. J. *Appl. Catal., B* **2001**, *31*, 183.
(43) Chakrabarty, D. K.; Rao, D. Y. *React. Kinet. Catal. Lett.* **1987**, *33*, 131.
(44) Voorhoeve, R. J. H.; Remeika, J. P.; Tribble, L. E. *Ann. N.Y. Acad. Sci.* **1976**, *272*, 3.
(45) Tascon, J. M. D.; Fierro, J. L. G.; Tejuca, L. G. *Phys. Chem.* **1981**, *124*, 249.
(46) Lou, H.; Zhen, H.; Yang, J.; Yao, Z.; Yu, S.; Ma, F. *Chem. J. Chin. Univ.* **1995**, *16*, 107.
(47) Yang, X.; Luo, L.; Zhong, H. *Appl. Catal., A* **2004**, *272*, 299.
(48) Teng, F.; Buergen, G.; Liang, S.; Zhu, Y. *Appl. Catal., A* **2007**, *328*, 156.
(49) Teng, F.; Xu, T.; Liang, S.; Buergen, G.; Yao, W.; Zhu, Y. *Catal. Commun.* **2008**, *9*, 1119.

JP711773W